Tuning the Physical Properties of Carboxylated Cellulose Nanocrystal (cCNC) Microspheres by Hybridizing with Silk Fibroin (SF)

Junqi Wu, Amelia Loesch-Zhang and Mark Andrews*

J. Wu, Prof. M. Andrews

Department of Chemistry, McGill University, 801 Sherbrooke St W, Montreal, QC, H3A 0B8, Canada

A. Loesch-Zhang

Laboratory of Macromolecular Chemistry and Paper Chemistry, Techniche Universitat Darmstadt, Alarich-Weiss-Str. 8, 64287 Darmstadt, Germany

E-mail : mark.andrews@mcgill.ca

A new class of hydrophobic/lipophilic cellulose microspheres are made from carboxylated cellulose nanocrystals (cCNC) by adding silk fibroin (SF) protein in the course of spray-drying from aqueous suspension. We found mere 2% SF addition could leverage the surface energy with an increase of contact angle from 27.5° to 60.4°. Besides the complete altered surface energy from cellulose beads, the hybrid SF-cCNC microspheres also show improved mechanical properties and prolonged diffusion kinetics for transporting water-soluble ions / molecules (e.g., methylene blue). Depth profiling of the SF-cCNC microspheres reveals that SF is more concentrated at the surface in comparison with the core, and this surface localization is the reason for the tuned properties. Moreover, post methanol treatment of the SF-cCNC hybrid microspheres induces a *β*-sheet phase transition to the Silk II structure, which can further enhance the mechanical properties and slow down the small molecule transport of the microspheres. Therefore, a new method has been established that could tune the physical properties of functional cellulose microspheres through the control of SF structural transformation, which could significantly benefit for controlled drug release and microplastic beads replacement applications.

1. Introduction

Microspheres in general play important roles in drug delivery,[1] cosmetics and skincare,[2] in florescent immunoassay,[3] as micro-carriers in biotechnology,[4] as viscosity modifiers,[5] stationary phases in chromatography,[6] and as abrasives.[7] The diversity of applications can be attributed to the many attractive features that can be built into microspheres, like variations in size, volume and specific surface area, versatility in microencapsulation techniques, regulated diffusion characteristics for molecule release and uptake, control over dispersibility, unique surface chemistry, and morphological complexity.[8] Increased consumer concerns regarding personal and environmental health have stimulated searches for sustainable and biodegradable microspheres; but it is not straightforward with those derived from natural sources like proteins and cellulose. This is because the mechanical, optical, and surface properties of these materials differ from those of conventional used microplastics, which were designed for functions that hydrophilic biopolymer were not. Nanocomposite microspheres can be a solution by incorporating new functional groups or new features without chemically modifying the biopolymers but to form stable microspheres.

Nanocomposite microspheres are usually prepared by aqueous polymeric solution mixing followed by emulsification method, heat induced sol-gel transition, solvent exchange, or freeze-drying.[9] Making biopolymer based nanocomposite microspheres usually starts with disassembling the molecular networks, and then mix the two polymers in solution. However, the crystalline structure of cellulose usually limits the cellulose dissolution, making it challenging to form cellulose-based nanocomposite microparticles. Carboxylated cellulose nanocrystals (cCNC) produced by catalyst-free aqueous hydrogen peroxide hydrolysis are alternatives to the specialty cellulosics from chemical dissolution. The process [10] developed to make cCNC has the advantages that H_2O_2 is used at concentrations below 10%, is fully consumed, simultaneously introduces the carboxylic acid group, produces primarily dilute sugars as easily disposable waste, conserves entropy (does not break up the cellulose crystal lattice), and yields cCNC that can be assembled into biodegradable microspheres or incorporate other biopolymer component to make composite microspheres.[11] cCNC can be a good candidate for making nanocomposite, because instead of dissolving the cellulose chains with harsh solvent conditions, CNC aqueous suspension can be directly used to incorporate other components in water.[12] It is also an unusual composition of matter because the nanorods nature of CNC (high crystallinity) when combining with dissolved biopolymer component and be

forced into a curved space (microsphere formation) can lead to structural transition that affects the distribution and property of the microspheres.

In this paper, we document the outcome of combining silk fibroin amorphous polymer chains with high aspect ratio carboxylated cellulose nanocrystals (cCNC) using spray drying to generate nanocomposite microspheres, where we discuss the adjustment of morphologies, mechanical properties, surface energy, and small molecule diffusion properties based on the compositions. Surprisingly, we found that building the nanocomposite from SF and CNC in microspheres lead to the formation of hydrophobic microspheres, which are made the first time with only non-covalent interactions, without surface chemical modification, and with 100% naturality.

We further used the well-known amorphous-to-β-pleated sheet transition to control the mechanical and surface properties of the nanocomposite microsphere. We used methanol to mediate the hydrophilic–lipophilic balance (HLB)[13] that is known to stimulate the organization of the silk protein chains. Amphiphilic SF consists of large hydrophobic H (heavy) chain and small hydrophilic L (light) chain regions, connected by a disulfide bond. The H chain comprises 12 repetitive domains consisting of clusters of oligo-peptides, Gly-Ala-Gly- Ala-Gly-Ser, [Gly-Ala]$_n$-Gly-Tyr, and [Gly-Val]$_n$-Gly-Ala (n = 1-8) separated by 11 amorphous peptide regions, mainly as Gly-Ala-Gly-Ser and Gly-Ala-Gly-Ala-Gly-Ser. The H chain contains considerable amounts of hydrophobic amino acid residues. Nevertheless, Ser and Tyr residues along the H chain are hydrophilic, while the charged glutamic acid (Glu) and asparatic acid (Asp) residues, are attributes that may confer polyelectrolyte character. We used spray-drying to produce the hybrid microspheres over a wide range of composition, with a view to rendering the microsphere both mechanically tunable and hydrophobic.

According to Griffin,[13] the hydrophilic-lipophilic balance value (HLB-value) is defined as the percentage ratio between the molecular weight of the hydrophilic group and the total molecule. In general, HLB values below 9 indicate surfactants in which lipophilicity dominates. For surfactants with HLB values above 11, hydrophilicity is larger than the lipophilicity. Surfactants with HLB values between 9 and 11 exhibit intermediate character. Tsukada *et al.* were among the first to document how aqueous methanol (HLB$_{methanol}$ ~10.6) induces $\alpha \rightarrow \beta$ conformational transitions in neat silk fibroin films.[14] This was followed by studies with ethanol[15] and small-molecule polyalcohols with different HLB values.[16] Alcohol induced structural transitions in SF have been reviewed.[17] The transformation of hydrophilic SF films to hydrophobic films can be induced by glycerol,[18] by blending with cellulose,[19] by tuning the casting

temperature,[20] and by crosslinking.[21] The transformations result from β-sheet formation, though the products can be diamorphic Silk I or II depending on processing conditions and solvent medium.[22] [23] Herein, we explored how building nanocomposites in a confined and curved space with the incorporation of high aspect ratio nanorods (CNC) affects the conformational transition of SF structure and its influence on HLB-value of the composite of matter.

In the following vibrational spectroscopic study, we examine structural transformations induced by methanol to delineate how the transformations are influenced by combining SF with cCNC in hybrid microsphere form via spray-drying. N1s XPS depth profiling reveals the distribution of SF in the cCNC in the microspheres. We evaluate how mechanical properties depend on the SF-cCNC ratio, evidence for enhanced hydrophobicity over the native cCNC microsphere, and the functional property of small molecule uptake and release. In the next section we first discuss the relation between microspheres morphology and the compositions.

2. Characterization of Hybrid Microspheres

Composition affects the morphology of the microspheres. We firstly explored how morphology changes when building nanocomposite using nanorods and amorphous polymer chains of SF with various compositions. **Figure 1** shows SEM images of cCNC microspheres, SF-cCNC hybrid microspheres, and SF microspheres. We spray dried particles over the range 100% cCNC, 2%, 5%, 10%, 20%, 50% SF in cCNC, to 100% SF. All suspensions were fixed at 0.5 wt % solids. From **Figure 1**, unadulterated (neat, 100%) cCNC microspheres emerged as roughly spherical particles that exhibited wrinkled surface texture. In this case, the average microsphere size was 1.89 μm, with broad 38.0% polydispersity. Incorporating 2% SF produced elongated, horseshoe and irregularly shaped particles. At 10% SF, we observed some donut shaped, collapsed hemisphere and irregular particles, but few elongated species. When the SF component was increased to 50%, we observed two strikingly different particle populations – smooth spherical particles (possibly inflated), collapsed blistered particles, set against a large population of much smaller irregularly shaped particles of considerable morphological variation.

The average particle size increased over the range 2% SF-cCNC (2.5 ± 0.8 μm) to 100% SF (7.5 ± 1.8 μm). We believe that particle size correlates with the size of water droplets before spray-drying, *i.e*, is related to the viscosity of water suspension when mixing different amounts of SF to cCNC. Equation 1[24] expresses the relation between droplet diameter and the feed solution properties such as surface tension, viscosity, and density.

$$D_d = K_f \cdot Q^n [\rho^a \cdot \gamma^b \cdot \mu^c] \tag{1}$$

Here D_d is the droplet diameter, Q is the feed solution volumetric flow rate, ρ is the density, γ is the surface tension, μ is the viscosity, K_f is an equipment constant, n is the flow rate, and a, b, and c represent the so-called power constants of solution properties. From the equation, the significant increase in the particle size for 100% SF may be related to increases in droplet diameter dominated by the high viscosity of the silk fibroin suspension, compared with that of cCNC. Spray-drying neat SF suspensions resulted in collapsed and broken shell particles. These may be due to internal bubble nucleation and collapse.

SEM provides information on the surface morphology of the microspheres. To examine the hollowness and internal porous structure of the microspheres, FIB-SEM was conducted on cCNC-SF microspheres with 2% and 20% SF content (Figure S1 and Figure S2). From the images, with the increase of SF content, the particles show a more porous internal structure. FIB milling studies provides another strategy to examine the impact of composition to the particle morphology.

3. How Spray-drying May Lead to Morphological Changes Depending on SF Content in cCNC Microspheres

We hypothesize that spray-drying plays a key role in leading to morphological changes in the nanocomposite system. In this session, we explain how the morphogical changes are dependent on spray-drying process. **Figure 1** emphasizes the broad range in particle morphology that arises when spray-drying cCNC, SF, and mixed suspensions of cCNC and SF. The morphology and size distribution of spray dried particles depends in complex ways on heat and mass transfer-related parameters. These have been elaborated in several publications concerned with spray-drying suspensions of solids.[25] Indeed, the parameter space for spray-drying suspensions of solids that gives rise to the diversity of particle shape and size distribution is an independent and lengthy study. In common practice, spray-drying process development is often empirical and experimentally driven. Nevertheless, given our own *fixed* spray-drying conditions (see Experimental), it is worth conjecturing about possible origins of the morphologies shown in **Figure 1**. We first note that particle formation is a non-stationary state event. The processes involving evaporation and solidification must be described by coupled nonlinear heat and mass transfer equations in the gas and the droplet, for which there are no analytical solutions. Our system has the added complexity that translational diffusion of cCNC rods differs from that of the protein, and that mixing and segregation of the two solidifying components must reflect

non-covalent cCNC-cCNC, cCNC-SF and SF-SF interactions as the droplet concentrates. In general, the structural categories for spray-dried particles will depend on the drying mechanism. Nevertheless, empirically, particle morphology can be related to process parameters through the dimensionless Péclet number, $P_e = \frac{R^2}{Dt_{dry}}$, where R is the droplet radius, t_{dry} is the drying time and D is the diffusion constant.[25g] P_e can be used to predict when a skin is likely to form. For low P_e, the diffusional velocity of the solute is faster or on the same order as the recession rate of the surface. In other words, diffusive transport is comparable to convective transport. Spherical or irregularly textured spherical particles can emerge. For large P_e, convective transport dominates over diffusive transport and spherical shell (internal void) particles and collapsed apricot-like particles can emerge. In other words, large Péclet numbers are associated with enrichment of the solute at the surface, which may lead to shell or skin formation. With this brief introduction, we turn to **Figure 1** and **Figure 2** for discussion.

Figure 2 (a) connects with **Figure 1** for 100% SF. SF is poorly soluble in pure water. In the range 0.1 to 0.7 wt %, the diffusion coefficient of silk fibroin varies from 2.4 to 1.3 x 10^{-12} m^2/s. As water evaporates upon spray-drying, SF diffuses to the water-air interface where the local viscosity increases, the protein reaches supersaturation, and SF precipitates, driving the droplet system from low Péclet number to larger Péclet. The high Péclet number system means that recession of the surface is fast compared with diffusion of the dissolved protein. Initially, we assume that SF is distributed homogeneously at the instant of water droplet formation. This creates a skin/shell structure as evaporation progresses. A sufficiently thick skin can maintain the shape of the particle while the remaining water diffuses through the shell or evaporates through openings or less dense regions of the shell. The resulting particles are hollow, and may collapse or wrinkle, depending on the thickness and mechanical properties of the skin. Indeed, the outlet (drying) temperature for the entire range of samples was maintained at 104 °C, *i.e*, above the boiling point of water. Since the outlet temperature exceeds the boiling point of water in the neat SF system, the pressure inside the evolving particle can exceed external pressure and the particle may inflate, burst and collapse. This is evident from **Figure 1** and **Figure 2** (a). Our finding for SF echoes that for spray-drying the small molecule, trileucene (L-Leucyl-L-Leucyl-L-Leucine).[25e] The poor solubility of trileucine pushes the otherwise low Péclet number to a value larger than 1. There is rapid surface accumulation of the phase-separated trileucine, resulting in a wrinkled, low-density particle resembling our SF microspheres. Under our spray-drying conditions, **Figure 1** also reveals that spherical, textured cCNC particles are produced by evaporating suspensions containing only cCNC. In **Figure 2** (b) the FIB cross-section of a

neat cCNC microsphere reveals a dense shell that circumscribes a porous or fibrous interior. Despite the large Péclet number for this system, collapse of the microsphere may be prevented by the hard, cCNC crust of the outer shell. Moreover, water evaporation may be impeded by formation of a cCNC gel phase as the cCNC nanocrystal concentration rapidly rises, a transition that might inhibit inflation and collapse of the particle. It is interesting that Peng *et al*. [25d] observe only donut shaped and irregularly shaped particles when *sulfated* CNC is evaporated from 1-2 wt % water suspensions at outlet temperatures between 93 and 84 °C, *i.e*, below the water boiling point.

Figure 1 shows that multicomponent spray-drying, by combining cCNC with 2 - 50% SF content, produced particles of heterogeneous morphology. It is tempting to attribute the morphological diversity to the addition of SF, but this glosses over the complex interplay of diffusion and aggregation of the two components. The literature on the origins of the morphological complexity that results from spray-drying multicomponent systems is just emerging.[25a] There is some evidence that addition hydrophobic lignin to sulfated cCNC increases the evaporation rate of water, but we see only scant evidence of the annular shaped particles reported by Zhu *et al*.[26] XPS evidence for accumulation of SF at the microsphere surface makes sense in view of the fact that during evaporation the hydrophobic protein will be driven to sequester at the air-water interface rather than remain homogeneously distributed within the particle. The literature on spray-drying frequently cites how diffusion (through the Péclet number, for example) impacts morphology when spray-drying mixtures of compounds, but interpretation of the data is difficult. The diffusion coefficients of sulfated CNC and SF are of the same order of magnitude in dilute regimes. The diffusion coefficient of SF is reported above. The translational diffusion coefficient of sulfated CNC varies with concentration[27] from about 0.2 to 7 x 10^{-12} m^2/s. Moreover, the cCNC diffusion coefficient can exhibit a significant entropic contribution should it enter the anisotropic liquid crystalline phase. XPS depth profiling (section 4) indicates that SF and cCNC appear to be intimately mixed within the 2 wt % and 20 wt % SF-cCNC microspheres. Rather than attribute homogeneity in the distribution of the cCNC and SF components to similar diffusion coefficients, we suggest that strong H-bonded interactions and component self-association may govern spatial uniformity. **Figure 2** (c) illustrates these remarks for the case that the multicomponent system yields a donut morphology.

4. Spatial Distribution of SF in SF-cCNC Hybrid System

We explored the spatial distribution of SF and cCNC in the microspheres via depth resolved XPS. A survey spectrum of SF revealed the major photoelectron peaks located at binding energy values of 531 eV, 400 eV and 285 eV, corresponding to O (1s), N (1s), and C (1s) atomic orbitals, respectively. Argon-ion projectiles were then used to remove successive layers between etching cycles.[28] We first calibrated etching depth and time. For cCNC microspheres, 10 min of etching with a current of 1.00 μA, 500 eV ion energy results in an etching depth of ~1 μm, or 0.1 μm/min. 2% SF-cCNC and 20% SF-cCNC microspheres were profiled, focusing on the elemental distribution of carbon, oxygen, and nitrogen. Then 10 cycles of etching were completed, gathering the element spatial profile after each etching cycle to collect subsurface information. Each etching cycled lasted ~5 min since the first measure did not include etching. **Figure 3** (a) - (c) and (e) - (g) show the carbon, oxygen, and nitrogen peaks for 10 etching sequences of 2% and 20% SF in cCNC, respectively. The etching process starts from the surface of the microspheres, and then penetrates ~5 μm into the densely packed microsphere sample over the total etching time. From **Figure 3** (d) and (h), it is evident that the surface of the microspheres is enriched in nitrogen, while the internal nitrogen content remains almost constant over the etching time. But the constant signal is due to etching through probably more than one layers of microspheres.

Published XPS data for neat silk fibroin powder reveals that registers nitrogen content typically on the order of 15.1%.[29] **Figure 3** (h) shows that we measure nitrogen about 14% N at the surface of a 20% SF-cCNC microsphere. This indicates that we have about 93% coverage by SF on the bead surface. Similarly, incorporation of 2% SF in cCNC results a surface nitrogen content of ~8%, showing a surface enrichment of about 53%. The spatial distribution of SF in cCNC means that spray-drying creates a type of hybrid core-shell microsphere, with SF enrichment in the shell layer. The hydrophobic shell (and the interior (see below)) provides a barrier to transport of aqueous solutes to the surface and then to the interior of the hybrid microparticle. In the next section we amplify the hydrophobic character by inducing conformational transitions of the SF *via* methanol treatment.

5. Hydrophobic/lipophilic properties of microspheres hybridized with silk fibroin

cCNC powders disperse well in water because they are hydrophilic, a property that originates from the abundance of hydroxyl, carboxylate or the carboxylic acid groups on the cCNC surface. Incorporation of SF to make SF-cCNC composite microspheres renders them hydrophobic and lipophilic. We compared the water contact angle of cCNC and 2% SF-cCNC

composite microspheres to measure the effect, and then examined their compatibility with an oil-in-water emulsion.

Contact angle measurement of powdered materials remains a challenge. Researchers have proposed several techniques to acquire contact angles on powders, frequently noting measurements on compressed materials.[62-64] Procedures include the sessile drop method on compacted pellets, and the Wilhelmy plate, AFM, and capillary pressure methods.[64] We chose the sessile drop method for simplicity, since we were interested in a comparative measure of hydrophilic/hydrophobic character rather than quantitative determination of surface energy. **Figure 4** (a) and **Figure 4** (b) show the contact angles of compacted cCNC and 2% SF-cCNC films by this method. We observed a significant increase in the contact angle from 27.5° for the cCNC pellet with no SF, to 60.4° for the 2% SF-cCNC pellet. This shows that incorporation of SF confers hydrophobic character.

Figure 4 (a) also reveals a degree of "creep" in the decreasing contact angle for cCNC as the pellet continually absorbs surface water. In contrast, the contact angle of the 2% SF-cCNC pellet was able to hold the water droplet for a comparatively longer period. We imaged the top of the pellet surface by SEM (**Figure 4** (c) and **Figure 4** (d)). As expected, the microspheres were "pancaked" by compression. The images reveal irregular open boundaries and holes between the flattened beads. These openings, and the process of crushing the microspheres, will change the surface energy and hence the wetting properties. While the results may not be a true reflection of the uncompressed powder, the contact angles measured for the SF doped and undoped samples are outside experimental error. The hydrophobic response of the SF-containing microsphere is consistent with their behavior in water-in-oil emulsions. This is described next.

6. Water-in-oil emulsion – Test of the Hybrid SF-cCNC Microsphere

Water-in-oil (W/O) emulsions are widely used in the cosmetics and food industries. When introducing microspheres in W/O emulsions, the microspheres need to be not only lipophilic to be stable in the oil phase, but they must also be hydrophobic so that they do not aggregate inside water droplets. In a cosmetic product, when water evaporates, the residual oil phase needs to be homogeneous in order to produce a fine film on the skin. When microspheres aggregate in the water phase, the homogeneity of the dried film is interrupted.

SF-cCNC microspheres in the range 2-10% SF in cCNC are both hydrophobic and lipophilic, making them candidates to replace microplastic beads that are used in W/O emulsion applications. **Figure 5** (b) shows that when pure cCNC microspheres are added to a W/O

emulsion, the cCNC microspheres immediately transfer to the water phase where they form large agglomerates. In contrast, the SF-cCNC microspheres of **Figure 5** (c) disperse uniformly and are stable over time (up to 2 years) in the oil phase.

The hydrophobicity of the SF-cCNC microspheres originates from the hydrophobic heavy (H) chains of the silk proteins. The amino-acid sequence of the L-chain is non-repetitive, forming hydrophilic and more elastic domains.[17] We now show that the SF-cCNC composite microspheres exhibit hydrophobic character because of the enrichment of hydrophobic domains on the surface of the microspheres.

7. Structural transitions in SF-cCNC microspheres by methanol treatment

Applications of silk fibroin rely widely on the formation of highly periodic crystalline regions in the protein. [17, 19b, 30] Adoption of the β-sheet conformational state changes mechanical and transport properties of materials made from silk fibroin and its composites. Infrared spectroscopy is one of the primary tools to interrogate the conformational transitions leading to β-sheet crystallinity in silk materials. The fractions of secondary structural components including random coils, α-helices, β-pleated sheets, turns, and side chains can be evaluated by careful spectral deconvolution. Here, we investigated how SF secondary structure is affected by spray-drying 2-component SF-cCNC suspensions, and how methanol treatment stimulates additional conformation relaxations. We selected Fourier spectral self-deconvolution signal processing to resolve the band contours that comprise the overlapped bands. With a high pass filter, broad and indistinct bands, like those of the amide I region of SF, are narrowed synthetically to yield deconvoluted spectrum with enhanced peak resolution.

The key carriers of spectroscopic information about chain conformation are absorption bands in the following regions: the amide I band (1600-1700 cm^{-1}, C=O stretching), amide II (1480-1575 cm^{-1}, N-H bending and C-N stretching) and amide III (1270-1230 cm^{-1}, C-N stretching and C=O vibration). In particular, the amide I peak in the range 1644 -1658 cm^{-1} can be used to confirm the extent to which fibroin adopts the silk I conformation. The amide I region comprises overlapping of the stretching vibrations ($v_{C=O}$) of pure C=O bonds in the protein backbones. The frequency of these vibrations is determined hydrogen bonding with the carbonyl groups, which directly reflect a particular secondary structure. It has been reported that organic solvents, mechanical stress, temperature, humidity, or the addition of other polymers can stimulate the conformational transition from silk I to silk II.[17] Silk II typically shows an amide I peak in the range 1620-1640 cm^{-1}.

10

Figure 6 (a) shows the vibrational spectra for different compositions of SF-cCNC microspheres before and after methanol treatment. Before methanol treatment, all compositions of SF-cCNC adopt the silk I structure. These transform to silk II with methanol treatment. **Figure 6** (b) confirms that in the amide I region, methanol treatment shifts the peak from 1651 cm^{-1} to 1627 cm^{-1}. Therefore, spray-drying and adding cCNC to the silk structure are not the only factors that determine conformational distribution. Methanol treatment plays a crucial role in this transformation.

We quantified the β-sheet formation before and after methanol treatment by Fourier self-deconvolution (FSD) of the FT-IR peak in amide I region.[30a, 31] The FSD curves contain tyrosine side chain, beta-sheet, random coil, alpha-helix, turns and beta aggregated strands in the amide I region. These are indicated in **Figure 6** (d). The peaks are marked as different colors: tyrosine side chains as orange, beta-sheet as green, random coils as blue, turns as cyan blue and alpha-helix as red.

We used the ratio of each peak area to the total amide I band area to quantify the amount of secondary structure in silk fibroin. **Figure 6** (c) shows the results of the percentage of *β*-sheet in SF-cCNC hybrid microspheres for different SF content from 2% to 50%, before and after methanol induced protein crystallization. Before methanol treatment, increasing the content of cCNC in the SF-cCNC microspheres is associated with higher *β*-sheet contribution to the spectra. Spray drying 100% silk fibroin quenches silk fibroin into its amorphous phase. It is possible that cCNC with SF in aqueous suspension prior to spray drying leads to mutual association between the two materials and some degree of *β*-sheet conformational change of the SF as it adsorbs onto nanocrystals. Not expectedly, methanol treatment of samples with increasing the SF content yielded greater content of the *β*-sheet.

We found that the duration of methanol treatment did not affect the maximum conversion to *β*-sheet, but the concentration of methanol solution did give a difference of *β*-sheet formation. (**Figure S3**, and **Figure S4**): exposure 20% aqueous MT induced a higher yield of *β*-sheet than did 80% aqueous MT. This effect is more significant for cCNC-SF microspheres then neat cCNC microspheres. The methanol exposure time was also monitored for *β*-sheet transition (**Figure S5** and **Figure S6**). The data shows a very fast *β*-sheet transition time (within 1 s) when treated with 80% methanol.

8. Small Molecule Uptake and Release

In our previous studies, we demonstrate the diffusion kinetics of methylene blue on cCNC microspheres, where we demonstrate how external factors like pH, ionic strength, and

temperature affect the diffusion.[11] Here, we intend to understand how hybridization and modification of cCNC microspheres with SF affect small molecule diffusions. We used the methylene blue (MB) dye molecule as a model compound to probe diffusion in the SF-cCNC microspheres. We compared the uptake/release (expressed as Q_t in mg dye/g microsphere) to those of neat cCNC microspheres to explore the impact of adding SF, before and after methanol treatment.

Figure 7 (a) shows the time evolution of MB uptake for 2% SF-cCNC microspheres. With neat cCNC microspheres, MB uptake is nearly instantaneous, and equilibrium is reached within 400 s (**Figure S7**). This finding corresponds closely to our previous observations for diffusion of MB in neat cCNC microspheres. After combining cCNC with SF, the rate of dye uptake decreased, requiring up to 1000 min to reach equilibrium. Notably, we observed no dye uptake before 200 min for either untreated and methanol treated SF-cCNC samples, for which the onset of uptake occurred at 200 min or approximately 300 min, respectively.

Methanol treated microspheres show slower dye uptake compared with the untreated SF-cCNC beads. This is consistent with enrichment in *β*-sheet conformations, increased crystallinity of the SF aggregates and enhanced hydrophobicity of the methanol treated particles (see next section). Our findings for the treated and untreated hydrophobic beads are in line with what we might expect by interpreting the transport of MB in the context of our reported film-pore diffusion model. In this two-resistance model, the first diffusion step requires that the dye overcome a diffusion barrier at the surface of a microsphere. This barrier regulates adsorption, which can be expressed in terms of an appropriate isotherm. We suppose that this barrier is dominated by the hydrophobic surface and that this is what delays the onset of diffusion compared with diffusion in the neat hydrophilic cCNC microsphere. The longer induction period for uptake in the hydrophobic particles may be related to the requirement for water diffuse into hydrophilic defects at the microsphere surface to render the bead more hydroplastic for penetration by MB. The second step can be described by Fickian diffusion of MB inside the pores of the SF-cCNC microsphere, but in this instance, the dye must move against the resistance created by the interior distribution of hydrophobic and crystalline domains of silk fibroin.

For MB release studies, we loaded neat cCNC, untreated 2% SF-cCNC, and methanol treated 2% SF-cCNC each with ~3.2 mg/g of MB. Near t=0, the release kinetics are very rapid for all three types of microsphere. This indicates a burst effect when MB molecules that are saturated on the surface of the microspheres are rapidly released to the solution. **Figure 7** (b) shows that

over time neat cCNC is most reluctant to release the dye. Hence, incorporating SF increased both the rate of release and the amount of dye released. We explain this as follows: cationic methylene blue dye may bind to cCNC particles in the microsphere through combinations of H-bonding and electrostatic interactions with the carboxylate anion. Controlled release of methylene blue from cCNC-based microspheres is regulated by the diffusion of MB through the porous interior and surface, a process that we have shown depends markedly on pH and ionic strength. The neat cCNC microsphere swells in neutral and high pH environments, an indication that water penetrates well into the structure. From the **Figure 5** XPS depth profiling study, SF creates a hydrophobic cage outside of the microspheres, which is more likely to hinder dye release when the particles are immersed in water. The contradictory results may suggest a redistribution of the SF and cCNC in water, leading to the surprisingly increase of the dye release.

Both the release rate and amount of release decrease after methanol treatment. This may be due to increases both to β-sheet crystallinity (physical barrier) and hydrophobicity.

9. Mechanical properties

Several methods are available to measure mechanical properties of microspheres. These include nanoindentation,[32] AFM force measurement,[33] and dynamic mechanical analysis compression.[34] Here we used microsphere colloidal probe nanoindentation to measure the Young's Modulus of the microspheres by AFM. (Reference submitted paper.) We compared the mechanical properties of cCNC and SF-cCNC microspheres with those of other types of microsphere. For petroleum-based beads, the Young's modulus varies from 2-8 GPa for polystyrene beads,[33] to 1-2 GPa for latex particles,[35] to 0.25-2 kPa for poly(acrylamide) microspheres.[36]

Figure 8 (a) plots the Young's modulus determined from the AFM force curve by fitting to the Hertz model. It is clear that with methanol treatment, there is a redistribution of the population of the microspheres such that a portion of them manifest larger Young's modulus compared with the untreated SF-cCNC beads. Neat cCNC microspheres have the lowest Young's modulus. Addition of 10% SF increases the stiffness of the SF-cCNC. This is visible as a shift in the bar graph to higher modulus. 10% SF microspheres exhibit a bimodal distribution of the Young's modulus with two maximums at approximately 30 MPa and 70MPa. This may indicate non-uniform distributions of silk fibroin and CNC within the microspheres, resulting in roughly two types of microspheres with different stiffness. 20% SF shows a similar bimodal distribution with two maximum at around 15 MPa and 50 MPa. Methanol treatment induces a shift in the

13

Young's modulus to higher values, an effect that is not surprising given the way that methanol enhances β-sheet conformations. This effect is observable for both 10% and 20% SF methanol treated samples. Beyond ~10% SF loading, further increases the amount of silk fibroin, say to 20%, decreases the stiffness of the microspheres. This may be the result of a plasticizing effect by the protein, making the microspheres more deformable.

10. Conclusions

A new type of hybrid microsphere has been developed by incorporating SF protein into cCNC via spray-drying. SF-cCNC microsphere morphology depends strongly on SF content under fixed spray-drying conditions. XPS depth profiling indicates that SF is concentrated on the surface of the microspheres, introducing hydrophobic and lipophilic character, attributed to the heavy chain hydrophobic domains in SF. AFM nanoindentation reveals that inclusion of SF up to 20% enhances the Young's modulus of the microspheres. The enhancement is linked to the quantity of β-pleated sheet conformations in the composite microsphere. Exposure of the hybrid beads to aqueous methanol increases the quantity of β-pleated sheet SF and further raises the stiffness of the particles. The quantity of β-pleated sheet conformations was determined by Fourier spectral deconvolution in the region of the amide I band of SF. Uptake and release of methylene blue probe molecule is inhibited by SF, compared with neat cCNC microspheres. The control over the small molecule transport properties makes them important in controlled drug delivery systems. The exhibition of hydrophobic and lipophilic properties, making them stable in water-in-oil emulsions and suggesting that the hybrid microspheres might be candidates to replace microplastic beads used in water-in-oil emulsions in cosmetics and personal care.

11. Experimental Section/Methods

11.1. Materials

Silk cocoons from Chinese *B. mori* silk were provided by Treenway silk (Lakewood, USA). Carboxylated cellulose nanocrystal (cCNC, 5.3 wt % solution in water) was obtained from Anomera Inc., Montreal, Canada. Na_2CO_3 (anhydrous) was from Fisher Scientific (Ottawa, Canada). LiBr (≥99%) was purchased from Sigma Aldrich (St. Louis, USA). Methylene blue (high purity) was obtained from Alfa Aesar (Heysham, UK). Methanol (HPLC grade) was purchased from Fisher Chemicals (Fair Lawn, USA), and acetone (99.6%) was purchased from Anachemica (Mississauga, Canada).

11.2. Degumming SF

14

SF was produced from silk cocoons following the procedure of *Rockwood et al.*[37] Cut cocoons (5 g) were added to a boiling solution of Na_2CO_3 (0.02 M, 2 L) where they were degummed for 30 mins. Afterward, degummed fibroin was rinsed in ultrapure water, and excess water was squeezed out. The residue was rinsed in water (1 L) for 20 mins (3 times), pressed and dried on aluminum foil overnight.

A solution of SF in LiBr (20 wt %) was prepared by pouring LiBr solution (9.3 M) on degummed SF and leaving the protein in an oven at 60°C for 4 h to dissolve. The resulting solution was dialyzed against water for 48 h, with a total of six times water changes. The solution was centrifuged twice at 4°C (9000 rpm, 20 min), decanted and stored at 4°C.

11.3. Spray-drying

Spray-drying was carried out with a Büchi Mini Spray Dryer B-191 (BUCHI Corporation, New Castle, USA) with inlet and outlet temperatures of 175 °C and 104 °C respectively, 30% pump speed and 70% aspirator. SF solution (SF, 2 wt %) was added to an aqueous suspension of cCNC sodium salt with vigorous stirring to obtain a homogenous suspension for spray-drying. cCNC microspheres containing 2 wt %, 5 wt %, 10 wt %, 20 wt %, and 50 wt % SF-cCNC were isolated as white free flowing powders.

11.4 Methanol Treatment

For methanol treatment, SF-cCNC microspheres (100 mg) were left overnight in an aqueous methanol solution (80 wt %, methanol 100 mL), filtered and then dried under vacuum .

11.5. SEM Imaging and Morphology Characterization

SEM was conducted using an FEI Quanta 450 Environmental Scanning Electron Microscope on samples with 3 nm platinum coating. Images were analysed with Fiji Image J open source image processing software (Copyright 2010-2020, Cambridge Astronomical Survey Unit). Particle diameters were measured with Image J and repeated for up to 100 particles. The particle diameter distribution was analysed using a Gaussian distribution function. Particle mean diameters were determined from the distribution analysis.

An FEI Helios Nanolab 660 DualBeam (Focused Ion Beam-Extreme High-Resolution Scanning Electron Microscope) was to image cCNC microspheres in cross-section. Samples were mounted on an aluminum SEM stub and coated with a 4 nm layer of Pt to enhance electrical conductivity. Milling of the sample was carried out with the FEI Helios Nanolab 660 DualBeam instrument (Thermo Fisher Scientific, Hillsboro, OR USA). After selecting a specific particle, a 2 μm thick layer of protective platinum stripe was deposited on the surface

of the region of interest to protect the surface from ion beam damage. Microsphere cross-sections were then prepared by gallium ion milling. A primary trench to clean the sample was milled at 30 kV ion beam accelerating voltage and 21 nA beam current. Following cleaning, cross-sections were obtained with beam current ranging between 9.3 nA to 0.79 nA. The smooth cross-section was imaged with an electron beam at an accelerating voltage of 2 kV, a beam current of 0.40 nA, and a working distance of 4 mm in the secondary electron mode.

11.6. Contact Angle Measurement

cCNC microspheres and 10% SF-cCNC microspheres powders were pressed into 1 cm diameter pellets. ~0.5 g of the cCNC or 10% SF-CNC microsphere powder was transferred into a recessed pellet mould. Microspheres were hydraulically pressed at 27.58 MPa load for 5 min. Pressure was applied slowly to prevent cracking of the pellet. Pellets of either cCNC or 2% SF-cCNC microspheres were used for sessile drop contact angle measurement. These were conducted with a Data Physics OCA 15EC goniometer and recorded with SCA software under ambient conditions. Under computer control, a water droplet of 5-7 µL was deposited on the pellet surface, and the contact angle measured within five seconds.

11.7. Water-in-Oil Emulsion

For water-in-oil emulsion preparation, the water phase was prepared by mixing water (6.2 g), with ethanol (95%, 0.4 g), NaCl (0.1 g), and Butylene Glycol (0.3 g). The oil phase was prepared by mixing C12-15 Alkyl Benzoate (2 g), KP 578 (silicone acrylate, 0.4 g), and KF-6038 silicone emulsifier, which comprises Lauryl PEG-9 polydimethylsiloxyethyl dimethicone (0.4 g). The oil phase was blended at 400 rpm until a homogeneous mixture was formed. The stirring rate was then adjusted to 500 rpm, and 0.2 g powder (cCNC microspheres or 10% SF-cCNC microspheres) was added and stirred until all the microspheres were dispersed well in the oil phase. The stirring rate was then adjusted to 800 rpm. The water phase was added dropwise to the oil phase. Once finished, the stirring rate was adjusted to 2500 rpm, and the mixture was stirred for 5 min until an emulsion formed. A blank sample was also prepared by replacing the powder by 0.2 g of water in the water phase. The final emulsions were cast as films on glass microscope slides. The dried films were observed under an optical microscope to determine the homogeneity of the emulsion system.

11.8. FTIR Spectroscopy and Deconvolution

Fourier transform infrared spectra were measured from SF-cCNC spray dried powders using ATR method in a Bruker ALPHA FTIR spectrometer (Bruker Optics Inc., Billerica, USA) with

single bounce diamond crystal and standard room-temperature LiTaO₃ MIR detector in the spectral region of 400 cm⁻¹ to 4000 cm⁻¹ using 60 scans with a nominal resolution of 4 cm⁻¹. Peak fitting was done using *OriginPro 2018b* software (OriginLab, Northampton, USA). Fourier self-deconvolution (FSD) was performed in the amide-I region (1580-1720 cm⁻¹). The second derivative was obtained from the original spectra in the amide I region with a nine-point Savitsky-Golay smoothing filter. The baseline correction is created based on the end points, both start and end to detect the baseline followed by application of the adjacent average smoothing method to reduce the noise. A simple linear interpolation is used to generate the baseline. Deconvolution was performed using Gaussian line shape with a half-bandwidth of 25 cm⁻¹ and a noise reduction factor of 0.3. Assignment of the eleven bands was reasoned from literature references.[31a] The resolved peaks were attributed to the different secondary structures of SF as follows: β-sheet at 1616-1637 cm⁻¹ (two peaks) and 1697-1703 cm⁻¹ (one peak); side chain aggregated strands: 1590-1615 cm⁻¹ (two peaks); random coils: 1638-1654 cm⁻¹ (two peaks); α-helices: 1655-1662 cm⁻¹ (one peak); and β-turns and bends: 1663-1696 cm⁻¹ (three peaks). Percentage contributions of the different secondary structures were calculated from the sum of the integrated peaks divided by the integral of the cumulative curve.

11.9. UV-Visible Spectroscopy Uptake and Release of Methylene Blue

Absorbance measurements to determine methylene blue uptake and release in SF-cCNC microspheres were conducted with a Thermo Scientific™ Evolution™ 260 Bio UV-Vis spectrophotometer (Fisher Scientific Company, Ottawa, Canada) and performed in the same way for both non-methanol treated and methanol-treated microspheres. For dye uptake, SF-cCNC microspheres (5 mg) were immersed in methylene blue solution (10 mg/L, 3 mL). The absorbance measurement was performed for 16 h, measuring every 10 min at the wavelength of 665 nm and a reference wavelength of 750 nm. For release monitoring, samples were prepared by immersing SF-cCNC microspheres (100 mg) in methylene blue solution (78 mg/L, 45 mL) overnight. The sample was filtered and washed with acetone. The measurement was conducted by immersing the dyed microspheres (5 mg) in water (3 mL). The release of methylene blue was measured by UV-vis spectroscopy for 72 h at a wavelength of 665 nm and a reference wavelength of 750 nm.

11.10. X-ray Photoelectron Spectroscopy (XPS)

XPS measurements were performed with a Thermo Scientific K-Alpha spectrometer. Binding energy values were calculated relative to the C(1s) photoelectron peak at 285.0 eV. An argon

ion gun with an energy of 500 eV and the low current (1.00 µA) was used for surface etching, which was performed for 300 s with 10 observation cycles. XPS was performed on each etching level with the flood gun on. The X-ray emission angle was 90 degrees with respect to the specimen surface. The diameter of the analyzed area was 400 µm. It was estimated that 10 min of etching corresponded to an etching depth of 1 µm. Spectra were deconvolved using Avantage Data System software with a combination of Gaussian and Lorentzian functions after background subtraction by the Shirley method, and the resulting curves attributed to the different types of bonds according to their binding energy. Integration of the obtained curves yielded the percent nitrogen content.

11.11. Mechanical Properties Measurement via AFM

A quantity of 10% SF-cCNC microspheres was dispersed in acetone and the mixture was cast on freshly cleaved, highly-oriented pyrolytic graphite (HOPG) substrate. The coating was dried under ambient conditions. Analysis was conducted under ambient conditions with a commercial AFM MFP-3D-BIO AFM instrument (Asylum Research, Santa Barbara CA). Biosphere B500-FM cantilevers (Nanotools, München, Germany) with an average spring constant of $k = 2.8$ N/m (determined by the thermal tune method) and a silicon colloidal bead tip radius of 500 nm were used for force measurement. Topographic images were acquired first to identify the SF-cCNC microsphere center positions and individual microsphere size. To investigate the mechanical properties of individual microspheres at well-defined location, the point-and-shoot method was used. After scanning an area coated with individual microspheres, approximately 100 of them were selected from the topographic image. A crosshair was used to select the center of a target microsphere for force curve collection. The mechanical properties of the microspheres were obtained by analyzing the force-distance curves according to the Hertz model. For force measurement, the contact mode was used with a trigger point of 2 V, a force distance of 1 µm, a scan rate of 0.99 Hz, and a velocity of 1.98 µm/s. For the topographic imaging, the AC mode was selected with a 20 µm scan size and 0.8 Hz scan rate. Some force curves were excluded when the results exhibited a Young's modulus indistinguishable from the substrate, meaning that the force curve was not measured for the microsphere surface. Similarly, points were rejected if the measurement yielded a stiffness too low, usually the result of lateral motion of the bead caused by a tangential force on the microsphere. This was tested by comparing topographic images of beads before and after indentation.

Supporting Information

Supporting Information is available from the Wiley Online Library or from the author.

Acknowledgements

References

[1]   N. K. Varde, D. W. Pack, *Expert Opinion on Biological Therapy* **2004**, 4, 35.

[2]   F. Casanova, L. Santos, *Journal of Microencapsulation* **2016**, 33, 1.

[3]   Y. Y. Go, S. J. Wong, A. J. Branscum, V. L. Demarest, K. M. Shuck, M. L. Vickers, J. Zhang, W. H. McCollum, P. J. Timoney, U. B. R. Balasuriya, *Clin Vaccine Immunol* **2008**, 15, 76.

[4]   W. Leong, D.-A. Wang, *Trends in Biotechnology* **2015**, 33, 653.

[5]   P. Khare, S. K. Jain, *AAPS PharmSciTech* **2009**, 10, 1295.

[6]   L. Qin, H. Wang, S. Liu, *Arabian Journal of Chemistry* **2017**, 10, S3515.

[7]   Y. Chen, Y. Wang, J. Qin, A. Chen, *Tribology Letters* **2015**, 58, 37.

[8]   Y. Yang, Z. Fang, X. Chen, W. Zhang, Y. Xie, Y. Chen, Z. Liu, W. Yuan, *Frontiers in Pharmacology* **2017**, 8.

[9]   J. Yang, J. Duan, L. Zhang, B. Lindman, H. Edlund, M. Norgren, *Cellulose* **2016**, 23, 3105.

[10]   T. M. Mark P. Andrews *Patent EP15826572.8A*, **2016**.

[11]   J. Wu, M. P. Andrews, *ACS Applied Nano Materials* **2020**, 3, 11217.

[12]   C. Li, J. Wu, H. Shi, Z. Xia, J. K. Sahoo, J. Yeo, D. L. Kaplan, *Advanced Materials* n/a, 2105196.

[13]   a) R. Pasquali, N. Sacco, C. Bregni, *Latin American Journal of Pharmacy* **2009**, 28; b) W. C. Griffin, *Journal of the Society of Cosmetic Chemists* **1954**, 5, 249.

[14]   M. Tsukada, G. Freddi, P. Monti, A. Bertoluzza, N. Kasai, *Journal of Polymer Science Part B: Polymer Physics* **1995**, 33, 1995.

[15]   X. Chen, Z. Shao, N. S. Marinkovic, L. M. Miller, P. Zhou, M. R. Chance, *Biophys Chem* **2001**, 89, 25.

[16]   S. Lu, J. Li, S. Zhang, Z. Yin, T. Xing, D. L. Kaplan, *Journal of Materials Chemistry B* **2015**, 3, 2599.

[17]   Y. Qi, H. Wang, K. Wei, Y. Yang, R.-Y. Zheng, I. S. Kim, K.-Q. Zhang, *Int J Mol Sci* **2017**, 18, 237.

[18]   P. Kuchaiyaphum, T. Yamauchi, R. Watanesk, S. Watanesk, *Applied Mechanics and Materials* **2013**, 446-447, 360.

[19]   a) S. Shang, L. Zhu, J. Fan, *Carbohydrate Polymers* **2011**, 86, 462; b) Y. Noishiki, Y. Nishiyama, M. Wada, S. Kuga, J. Magoshi, *Journal of Applied Polymer Science* **2002**, 86, 3425.

[20]   O. N. Tretinnikov, Y. Tamada, *Langmuir* **2001**, 17, 7406.

[21]   S. Zhao, R. He, X. Zhang, W. Zeng, T. Zhang, W. Yu, H. Liu, *Textile Research Journal* **2019**, 89, 3811.

[22]   X.-J. Lian, S. Wang, H.-S. Zhu, *Frontiers of Materials Science in China* **2010**, 4, 57.

[23]   C. Guo, C. Li, D. L. Kaplan, *Biomacromolecules* **2020**, DOI: 10.1021/acs.biomac.0c00090.

[24]   A. C. M. Daniel Santos, Vitor Sencadas, José Domingos Santos, Maria H. Fernandes and Pedro S. Gomes, in *Biomaterials - Physics and Chemistry - New Edition*, DOI: 10.5772/intechopen.72247 (Ed: R. P. a. T. Musumeci), IntechOpen **2017**.

[25]   a) A. B. D. Nandiyanto, K. Okuyama, *Advanced Powder Technology* **2011**, 22, 1; b) D. E. Walton, C. J. Mumford, *Chemical Engineering Research and Design* **1999**, 77, 442; c) D. Walton, *Developments in Chemical Engineering and Mineral Processing* **2002**, 10, 323; d) Y. Peng, Y. Han, D. J. Gardner, *Wood and Fiber Science* **2012**, 44, 448; e) R. Vehring, W. R. Foss, D. Lechuga-Ballesteros, *Journal of Aerosol Science* **2007**, 38, 728; f) J. Vicente, J. Pinto, J. Menezes, F. Gaspar, *Powder technology* **2013**, 247, 1; g) A. Osman, L. Goehring, A. Patti, H. Stitt, N. Shokri, *Industrial & Engineering Chemistry Research* **2017**, 56, 10506; h) D. E. Dobry, D. M. Settell, J. M. Baumann, R. J. Ray, L. J. Graham, R. A. Beyerinck, *Journal of pharmaceutical innovation* **2009**, 4, 133.

[26]   Z. Zhu, S. Fu, L. A. Lucia, *ACS Sustainable Chemistry & Engineering* **2019**, 7, 5376.

[27]   J. Van Rie, C. Schütz, A. Gençer, S. Lombardo, U. Gasser, S. Kumar, G. n. Salazar-Alvarez, K. Kang, W. Thielemans, *Langmuir* **2019**, 35, 2289.

[28]   J. B. Gilbert, M. F. Rubner, R. E. Cohen, *Proceedings of the National Academy of Sciences* **2013**, 110, 6651.

[29]   J. Shao, J. Liu, J. Zheng, C. M. Carr, *Polymer International* **2002**, 51, 1479.

[30]   a) S. Y. Cho, M. Abdulhafez, M. E. Lee, H.-J. Jin, M. Bedewy, *ACS Applied Nano Materials* **2018**, 1, 5441; b) J. Kundu, R. Mohapatra, S. Kundu, *Journal of Biomaterials Science, Polymer Edition* **2011**, 22, 519.

[31]   a) X. Hu, D. Kaplan, P. Cebe, *Macromolecules* **2006**, 39, 6161; b) P. Amornsudthiwat, M. Nitschke, R. Zimmermann, J. Friedrichs, K. Grundke, K. Pöschel, S. Damrongsakkul, C. Werner, *Biointerphases* **2015**, 10, 029509.

[32]   M. Küçükoflaz, B. Saraçoğlu Kaya, M. O. Caglayan, *Polymer-Plastics Technology and Materials* **2019**, 58, 765.

[33]   D. Guo, J. Li, G. Xie, Y. Wang, J. Luo, *Langmuir* **2014**, 30, 7206.

[34]   J. Kajtna, U. Šebenik, *International Journal of Adhesion and Adhesives* **2017**, 74, 100.

[35]   S. Tan, R. L. Sherman, W. T. Ford, *Langmuir* **2004**, 20, 7015.

[36]   N. R. Labriola, E. Mathiowitz, E. M. Darling, *Biomater Sci* **2016**, 5, 41.

[37]   D. N. Rockwood, R. C. Preda, T. Yücel, X. Wang, M. L. Lovett, D. L. Kaplan, *Nature Protocols* **2011**, 6, 1612.
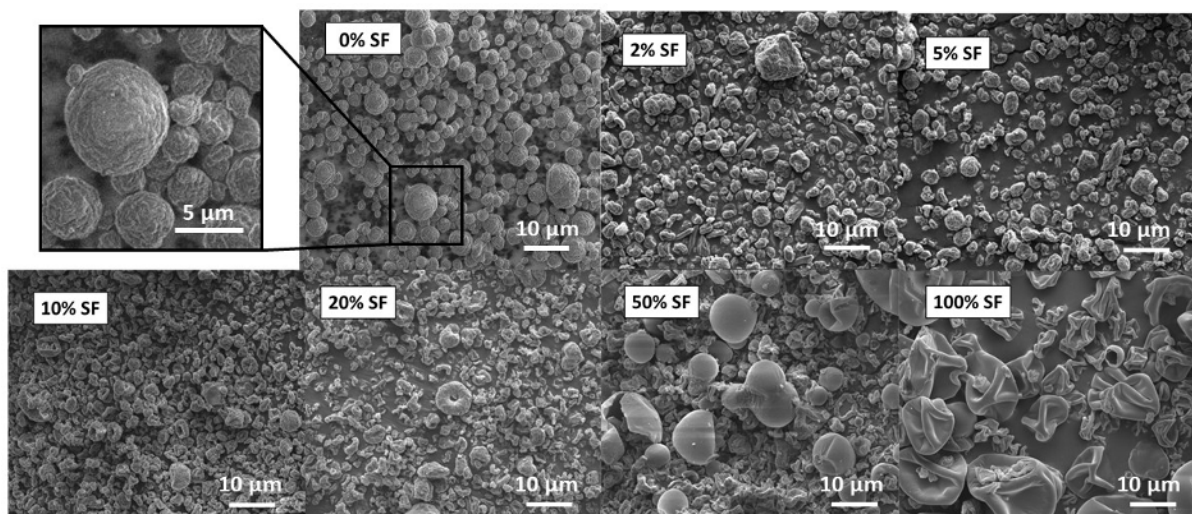
Figure 1. SEM images of cCNC microspheres. From left to right and top to bottom, increasing SF content.
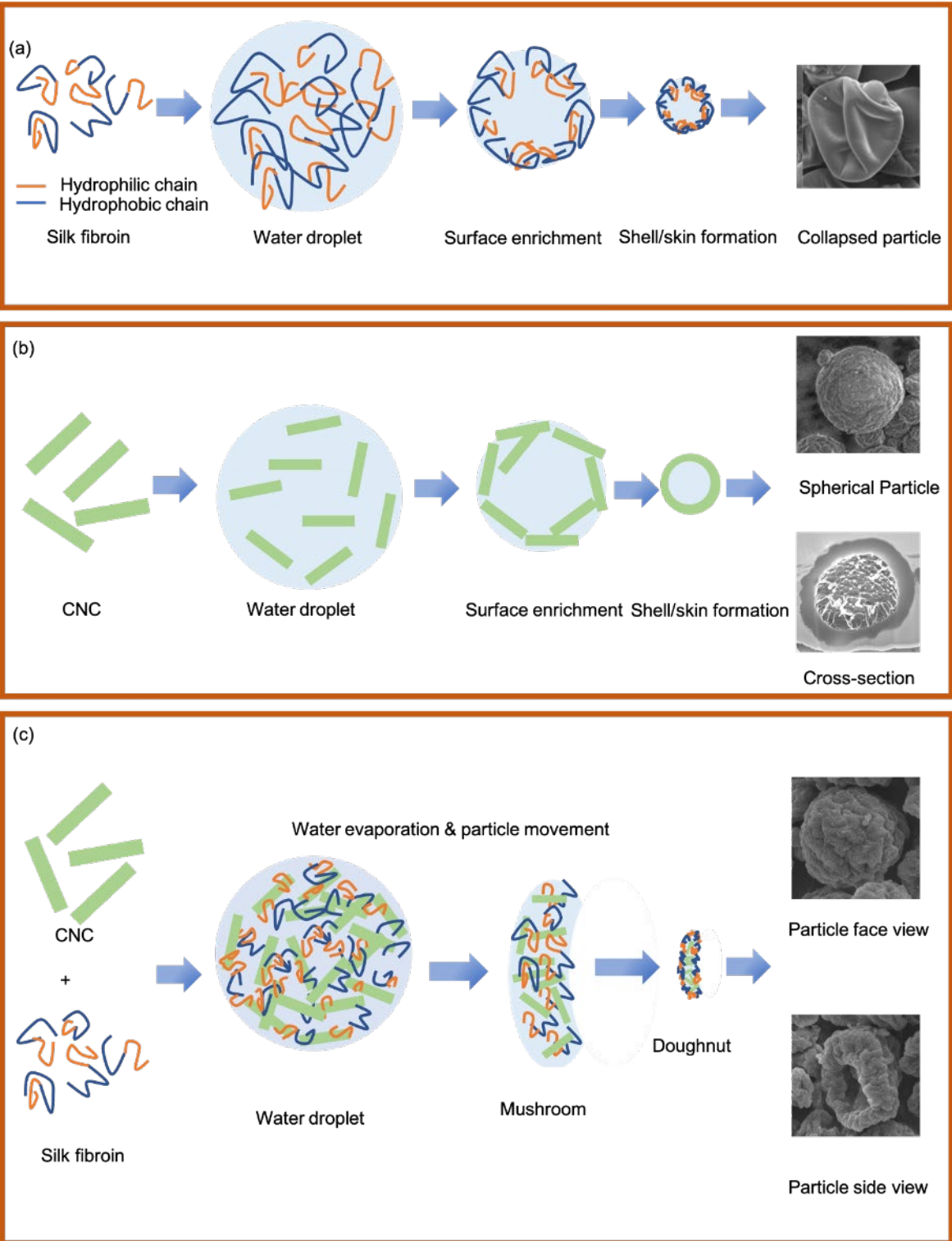
Figure 2. Illustrations of possible microsphere formation mechanisms *via* spray-drying. (a) Spray-drying SF water suspension leads to collapsed particles. (b) Spray-drying cCNC water

suspension leads to spherical particles with a dense shell and porous interior. (c) Spray-drying cCNC and SF mixtures may lead to donut-shaped particles.
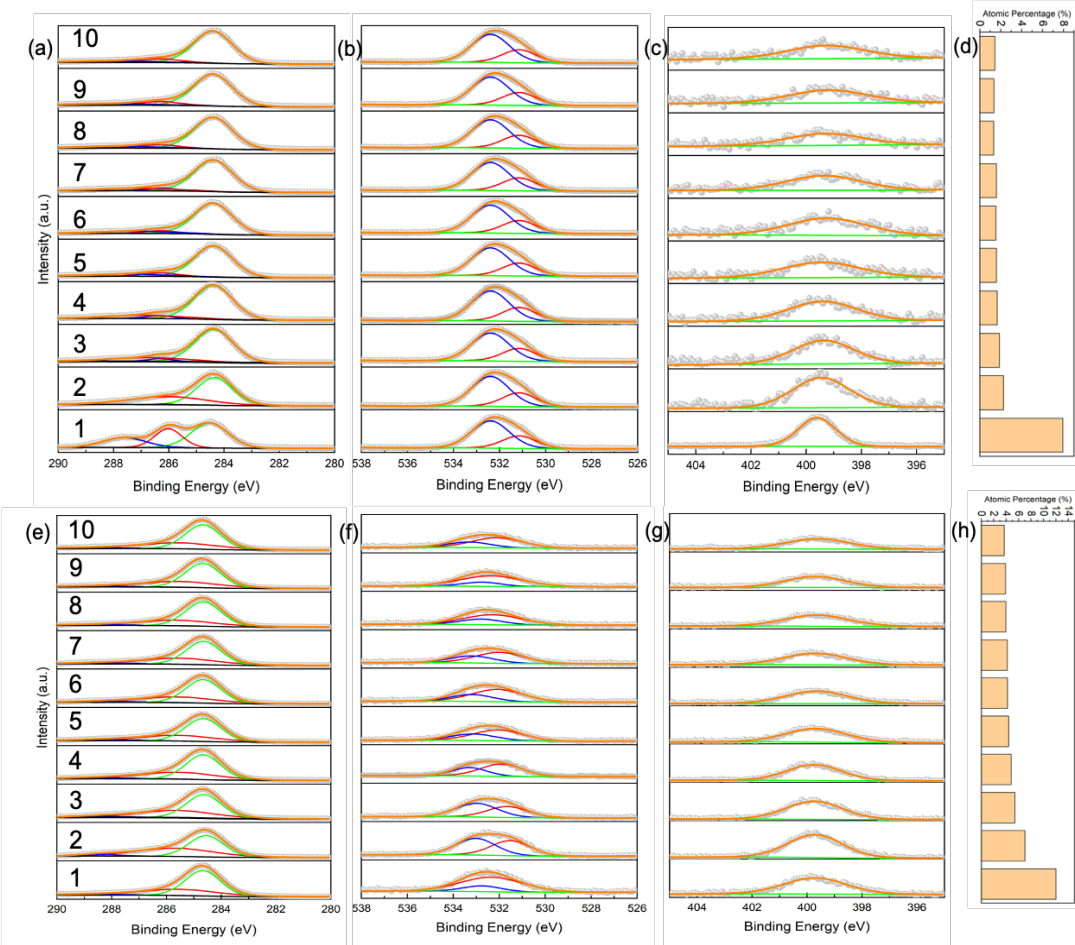

Figure 3. XPS depth profile of 2% SF-cCNC microspheres (a-c) and 20% SF-cCNC microspheres (e-g) for C 1s (a), O 1s (b) and N 1s (c) peaks for 10 etching sequences over a total etching time of 5 min. The histogram (d) shows the decreasing % nitrogen located from the bead surface to the interior over 10 successive etching sequences for 2% SF-cCNC microspheres. The histogram (h) shows the % nitrogen located from the bead surface to the interior over 10 successive etching sequences for 20% SF-cCNC microspheres.
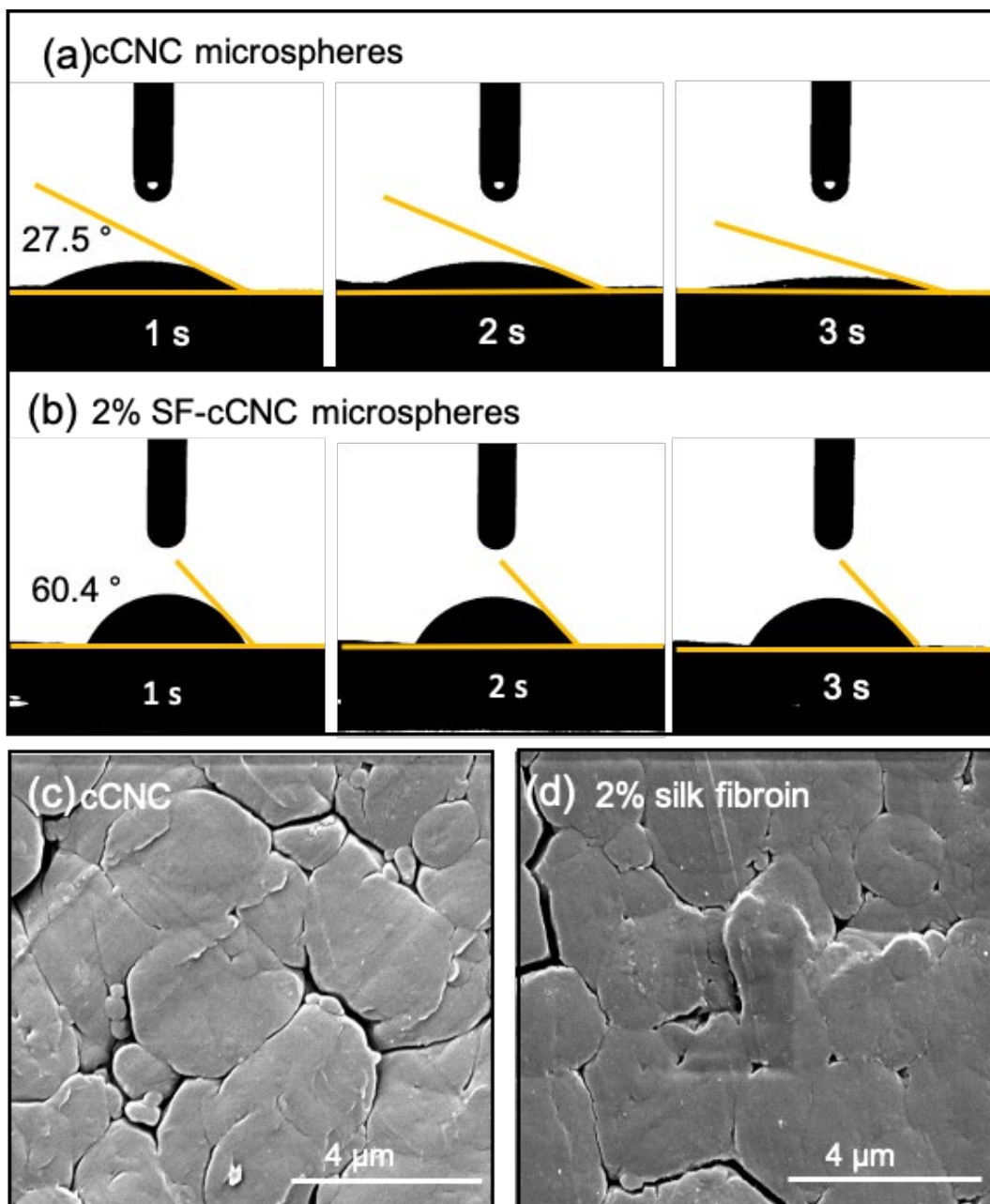
Figure 4. Sessile drop contact angle measurement of pelletized cCNC and 2% SF-cCNC microspheres. The needle tips are visible poised above the water droplets that are delivered under computer control. The microspheres pressed into flat pellets, visible in (a) and (b) as the black rectangular substrate where the water droplet sits. (a) Contact angle on pellet of cCNC microspheres at 1 s, 2 s, and 3 s elapsed time. (b) Contact angle of pellet from 2% SF-cCNC microspheres at 1 s, 2 s, and 3 s elapsed time. (c) SEM image of the surface of the pelletized cCNC microspheres. (d) SEM image of the surface of the pelletized 2% SF-cCNC microspheres.
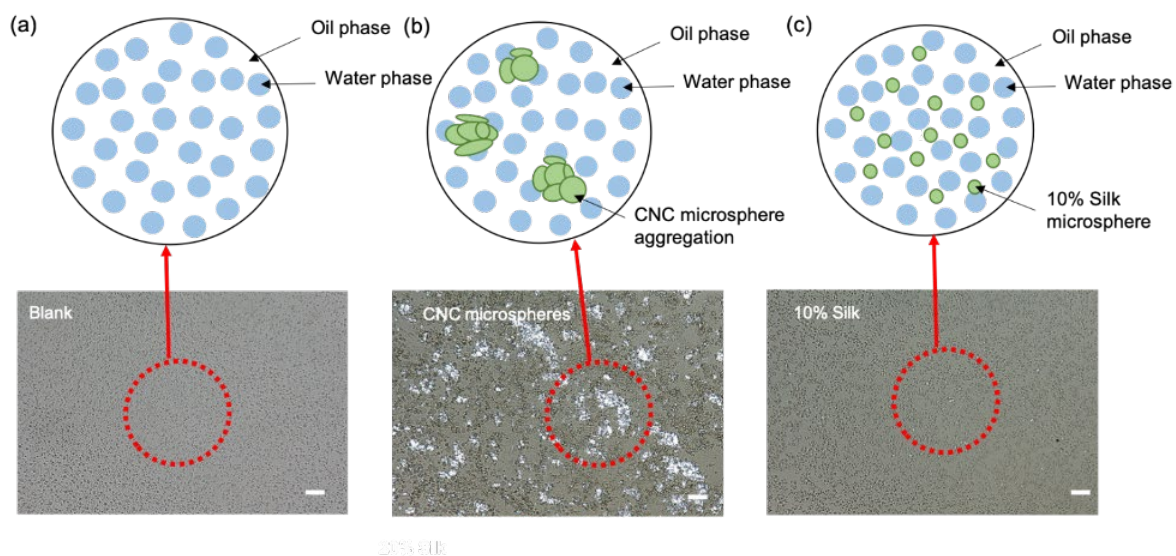
Figure 5. Comparison of cCNC microspheres and SF-cCNC microspheres in water-in-oil (W/O) emulsions. (a) W/O emulsion and optical microscope image of the emulsion as a film on a glass substrate. (b) Optical micrograph of cCNC microsphere aggregation in the water phase in a film on a glass substrate. (c) Optical micrograph of 10% SF-cCNC microspheres homogenously distributed in the same W/O emulsion as a film on a glass substrate. Scale bar: 30 μm

Green: β-Sheet Red: α-helix Blue: Random coil Orange: Side chains Blue: Turns
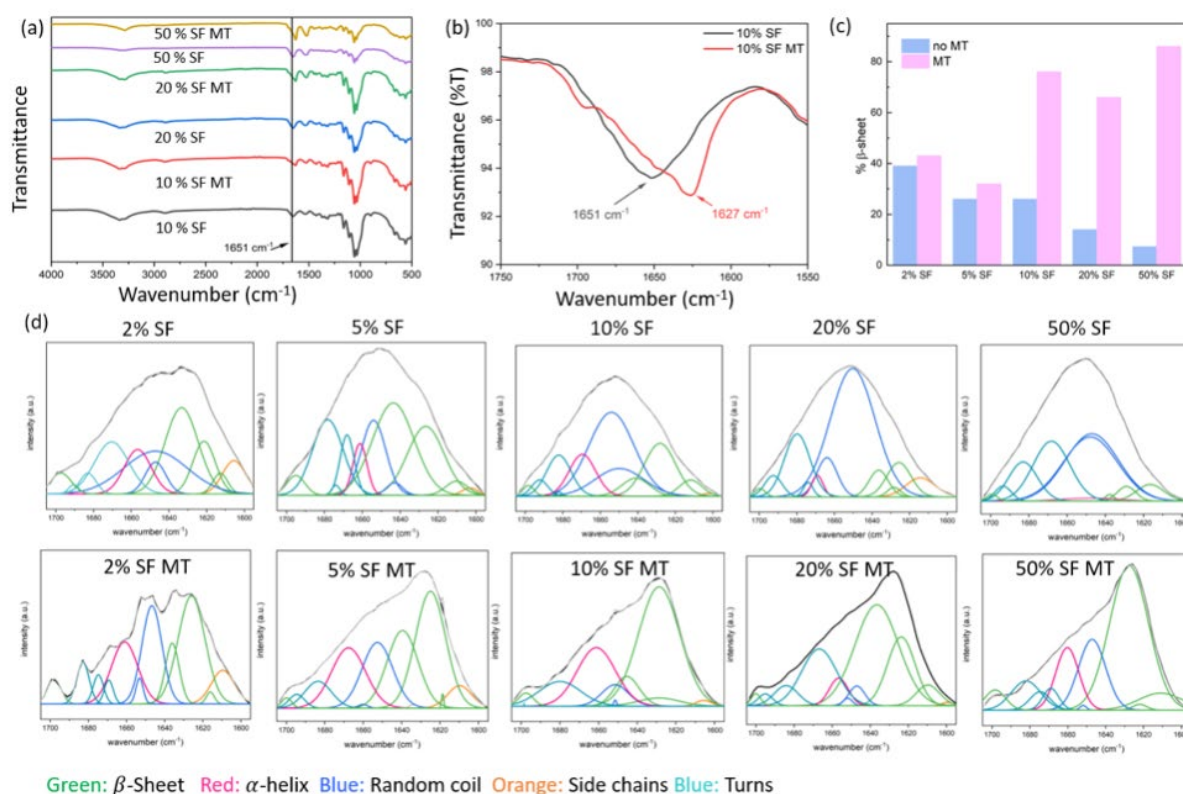
Figure 6. FT-IR spectra of SF-cCNC microspheres. **(**a) FT-IR spectra of SF-cCNC microspheres as functions of SF content in the microsphere, before and after methanol treatment. The solid vertical line locates the position of the amide I band. (b) FTIR spectra in the amide I region for 10% SF-cCNC microspheres before and after methanol treatment showing the shift of the amide I peak. (c) Percentage contribution of the **β**-sheet conformation, before and after methanol treatment, as a function of the composition of SF-cCNC microspheres. (d) Fourier self-deconvoluted spectra of SF-cCNC microspheres in the amide I region. The colored peaks are identified by their spectral contributors beneath the spectra in (d).
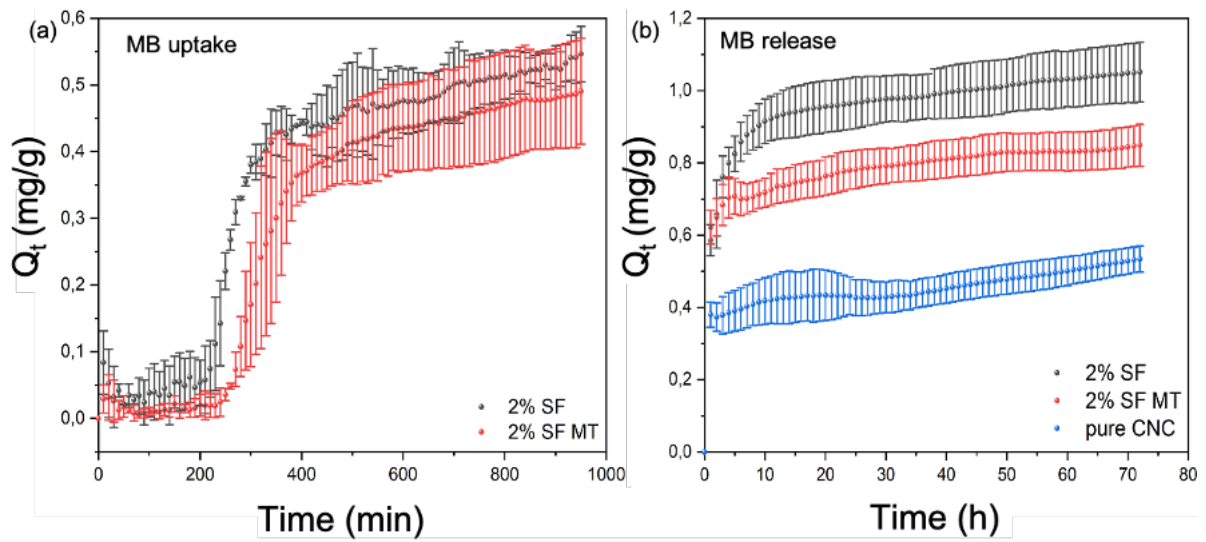
Figure 7. Methylene blue dye mass transfer in cCNC and SF-cCNC microspheres. (a) Methylene blue dye adsorption kinetics for 2% SF-cCNC microspheres before and after methanol treatment (MT). (b) Methylene blue dye release kinetics for 2% SF-cCNC microspheres before and after methanol treatment compared with neat cCNC microspheres.
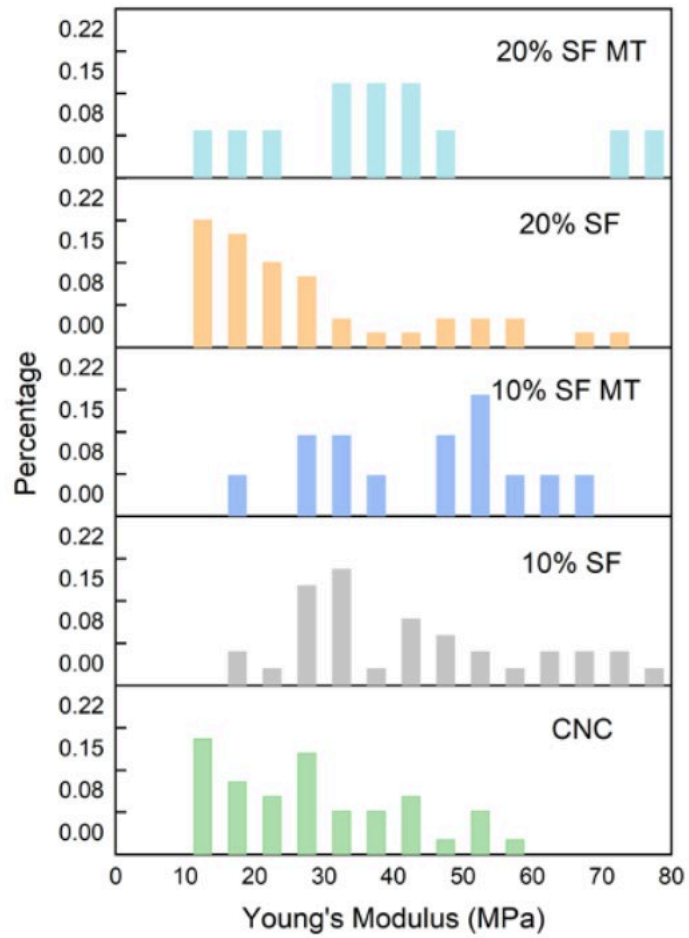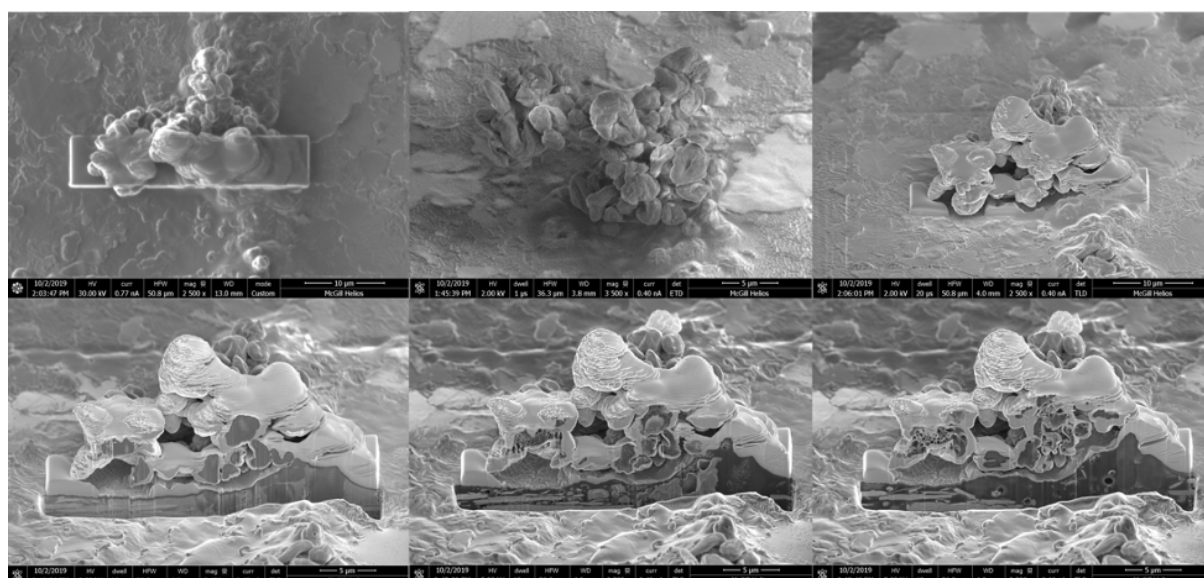
Figure 8. Young's Modulus comparison of cCNC, 10% SF-cCNC, and 20% SF-cCNC before and after methanol treatment. (N_{CNC}=46, $N_{10\%SF}$=52, $N_{10\%SFMT}$=31, $N_{20\%SF}$=50, $N_{20\%SFMT}$=24)

Supporting Information

Tuning the Physical Properties of Carboxylated Cellulose Nanocrystal (cCNC) Microspheres by Hybridizing with Silk Fibroin (SF)

*Junqi Wu, Amelia Loesch and Mark Andrews**

**Figure S1.** FIB-SEM milling to reveal internal structure of 2% SF-cCNC microspheres.
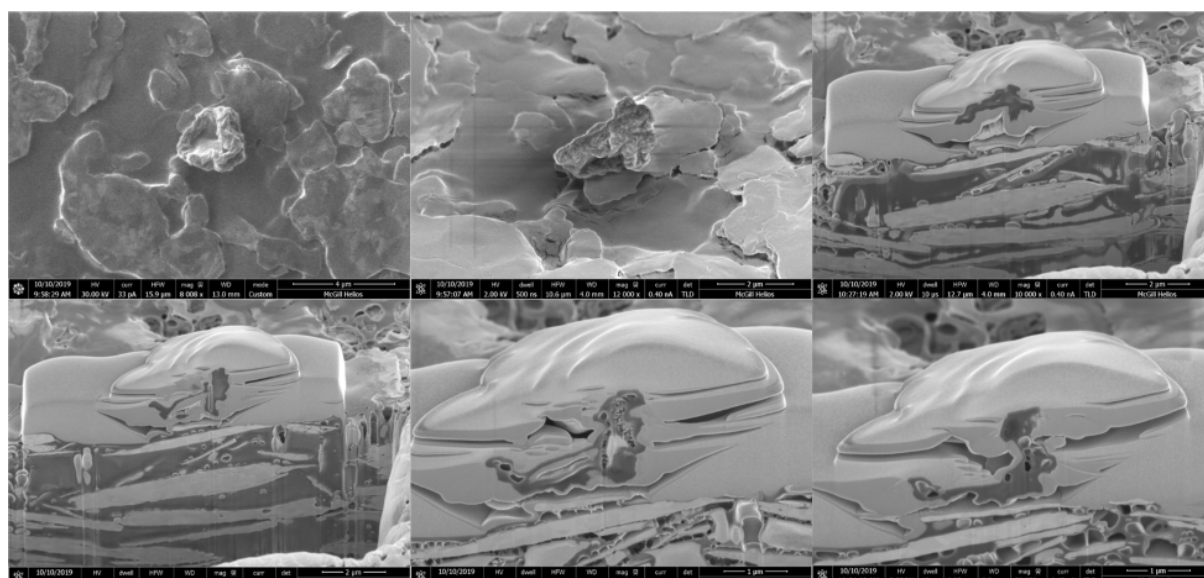
Figure S2. FIB-SEM milling to reveal internal structure of 2% SF-cCNC microspheres
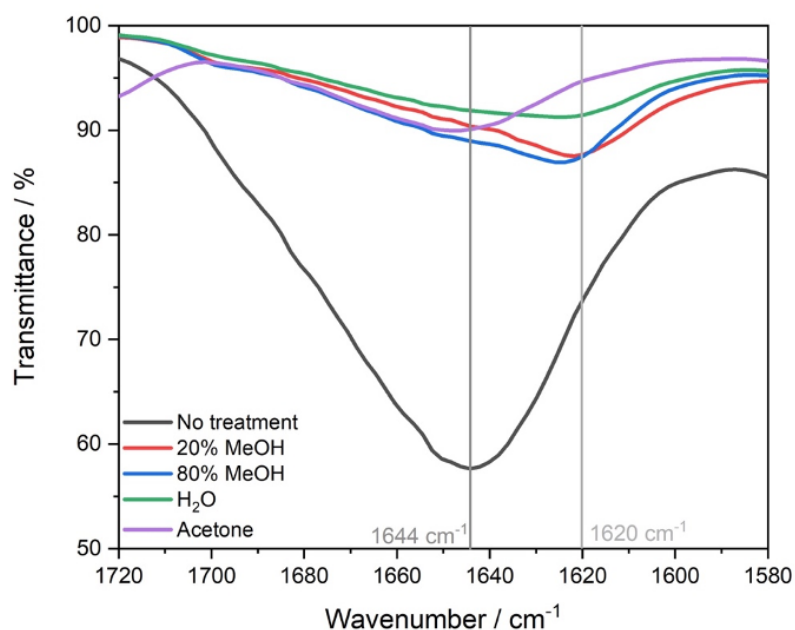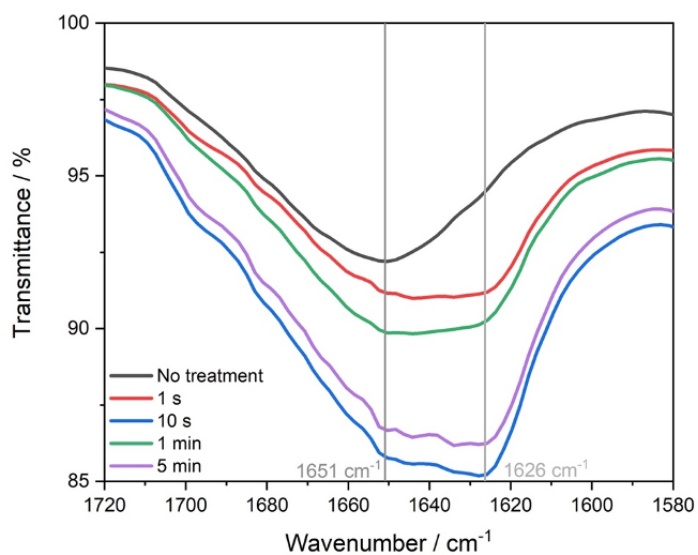
Figure S3. Evolution of amide bond stretching region of 10 % SF-cCNC microspheres after treatment with aqueous methanol, water and acetone compared with an untreated sample.
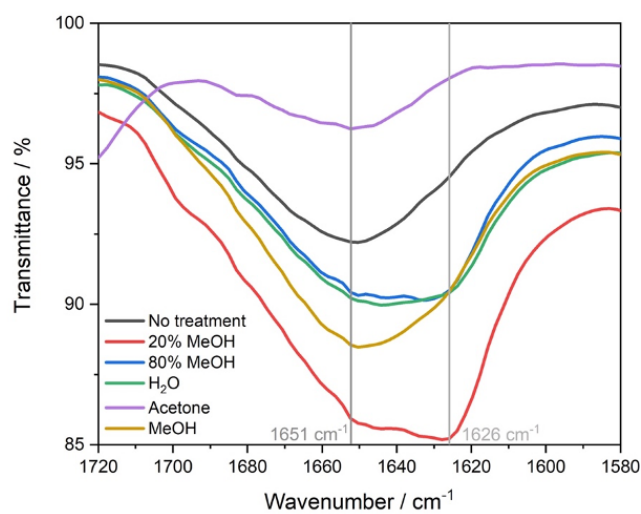

Figure S4. Evolution of amide bond stretching region of 20 % SF-cCNC microspheres after treatment with neat methanol, aqueous methanol, water and acetone compared with an untreated sample.
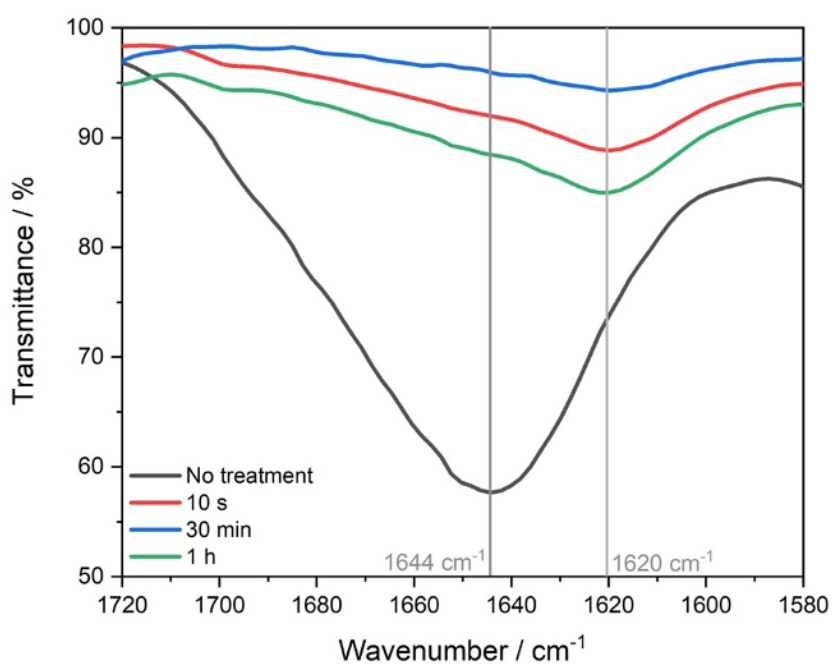
Figure S5. Time evolution of amide bond stretching region of 10 % SF-cCNC microspheres after treatment with 80% methanol compared with an untreated sample.

Figure S6. Time evolution of amide bond stretching region of 20 % SF-cCNC microspheres after treatment with 80% methanol compared with an untreated sample.
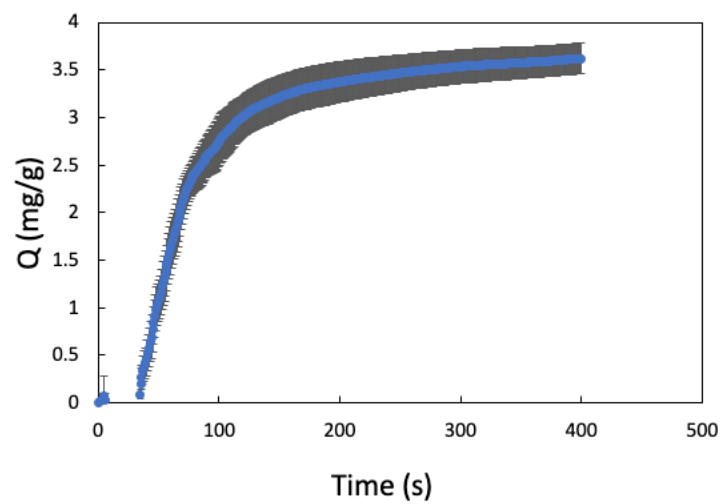
Figure S7. Dye uptake kinetics of cCNC pristine microspheres at room temperature in methylene blue solution.